Equilibria between Ionophore A23187 and Divalent Cations: Stability of 1:1 Complexes in Solutions of 80% Methanol/Water†

Clifford J. Chapman,‡ Anil K. Puri,‡ Richard W. Taylor,§ and Douglas R. Pfeiffer*,‡

The Hormel Institute, The University of Minnesota, Austin, Minnesota 55912, and Department of Chemistry, University of Oklahoma, Norman, Oklahoma 73019

Received December 29, 1986; Revised Manuscript Received April 10, 1987

ABSTRACT: The cation complexation equilibria between ionophore A23187 and several alkaline earth and first transition series divalent cations have been investigated. Absorption and fluorescence spectroscopy were used to monitor the reactions which were studied in solutions of 80% methanol/water, at 25 °C, and under conditions of controlled ionic strength and pH*. Titration of the ionophore with divalent cations results first in formation of the dimeric species MA_2 and subsequently in the formation of MA^+ by disproportionation of the first product. With Zn^{2+}, Ni^{2+}, and Co^{2+} (above pH* ~6), a third species is detected which is postulated to be MA·OH. The existence of this species with Mn^{2+} and alkaline earth cations is uncertain. For formation of MA_2, the second stepwise stability constant is similar to or exceeds the first value with all cations studied. However, it is possible to isolate the first reaction and determine accurate stability constants by working at an ionophore concentration of 3×10^{-8} M or less and by employing pH* values which preclude interference by the mixed ionophore/hydroxide species. Under these conditions, the relationship between log K_{MA}' and pH* is linear and displays a slope of 1.0. pH*-independent stability constants were calculated by using pH*-dependent stability constants and the known value of the ionophore's protonation constant in this solvent. The logarithms of the values obtained ranged from 7.54 ± 0.06 for Ni^{2+} to 3.60 ± 0.06 for Ba^{2+}. The selectivity sequence and relative affinities (in parentheses) for the species MA^+ are as follows: Ni^{2+} (977) > Co^{2+} (331) > Zn^{2+} (174) > Mn^{2+} (34) > Mg^{2+} (1.00) ≃ Ca^{2+} (0.89) > Sr^{2+} (0.20) > Ba^{2+} (0.11). Data are discussed in comparison to other studies on the complexation properties of A23187 and in terms of their significance to interpreting the transport properties of this ionophore.

The antibiotic A23187 (see Figure 1 for structure) was isolated (Hammill et al., 1972) and shown to be an ionophore for divalent cations (Reed & Lardy, 1972) approximately 15 years ago. This compound is now used routinely to manipulate Ca^{2+} ion concentration gradients across the membranes of cells, subcellular organelles, and artificial membrane preparations. As with other ionophores, it is common to attribute the biological and biochemical effects of A23187 to its classical activity (the transmembrane exchange of Ca^{2+} for $2H^+$) without fully considering whether other complexation or transport properties of the compound could be contributing to the results. This situation pertains, in part, because the chemical properties of this and other ionophores, which underlie their transport activities, have not been thoroughly studied [see Taylor et al. (1982) for a review].

To improve the general understanding of ionophore-catalyzed cation transport and to allow more detailed interpretation of the biological activities of A23187, we have been investigating the component, sequential reactions which compose the ionophore's transport cycle (Pfeiffer et al., 1978). Figure 1 illustrates the component reactions and their sequence which constitute the current model. To apply this model to the description and analysis of the ionophore's transport activities, it is necessary, as a minimum, to know the equilibrium and kinetic (or diffusion) constants for each of the individual steps. Additional information of value includes the understanding of how selected chemical forms of the ionophore interact with and diffuse across phospholipid bilayer membranes and the determination of how ionophore–membrane interactions affect the properties of the cation complexation–decomplexation reactions. Previous work in these areas includes studies on the acid–base properties of A23187 (Kauffman et al., 1982), studies on the monovalent cation binding properties of this ionophore (Taylor et al., 1985), investigations into the interactions of the species HA and A^- with phospholipid vesicles (Kauffman et al., 1983), and similar studies by other investigators (Tissier et al., 1979, 1985; Albin et al., 1984). In the present report, we are extending this work to include solution equilibrium studies with divalent cations.

Materials and Methods

Methanol/Water Solvents. Solutions of 80% methanol in water (w/w) were prepared gravimetrically. This solvent composition was selected because previous work has shown that A23187 in 80% methanol/water displays protonation and monovalent cation equilibrium complexation constants which are very similar to those obtained with the membrane-associated ionophore (Kauffman et al., 1982, 1983; Taylor et al., 1985). The methanol utilized was reagent grade and was distilled from zinc dust and potassium hydroxide shortly before use. The water utilized was distilled, deionized, and had a specific resistance of approximately 13 MΩ-cm. Unless otherwise specified, methanol/water solutions contained the following solutes: 33 mM tetraethylammonium perchlorate, 5 mM 2-(*N*-morpholino)ethanesulfonic acid (Mes),[1] 5 mM

† Supported in part by U.S. Public Health Service Grant GM-24701 from the National Institutes of Health, by U.S. Public Health Service Grant HL 08214 from the Program Project Branch, Extramural Programs, National Heart, Lung, and Blood Institute, by U.S. Public Health Service Training Grant HL 07311, and by The Hormel Foundation.

* Correspondence should be addressed to this author.

‡ The University of Minnesota.

§ University of Oklahoma.

0006-2960/87/0426-5009$01.50/0

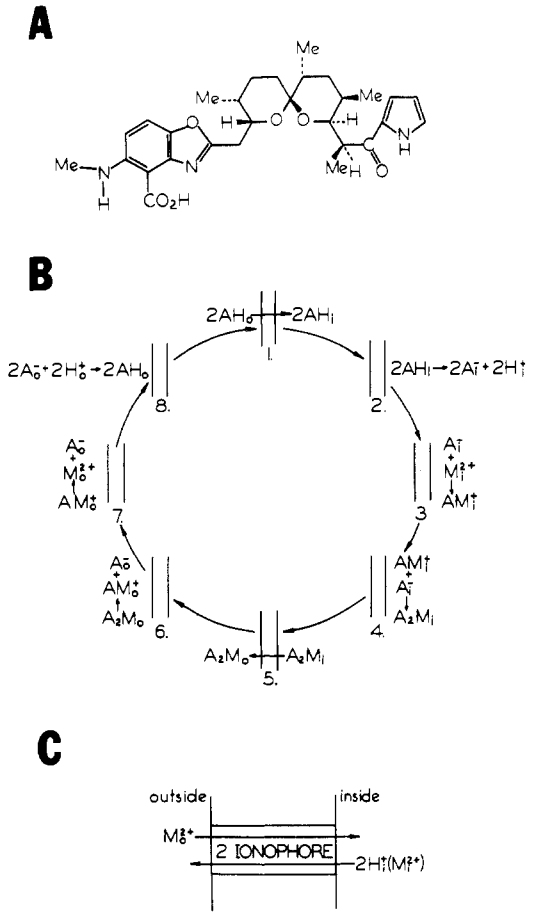

FIGURE 1: Structure and transport reaction of ionophore A23187. (A) The structure of the ionophore as originally reported by Chaney et al. (1974). (B) The minimum number of sequential component reactions required to complete one cycle of divalent cation transport by A23187. The pairs of verticle lines shown in each step of the cycle are meant to illustrate the phospholipid bilayer membrane across which transport is occurring. The subscripts "i" and "o" associated with the various chemical species refer to location as inside or outside of the membrane, respectively. (C) The overall transport reaction of A23187 exchanging a divalent cation for $2H^+$, via the dimeric complex. When the reactions in (B) are summed, they equal the overall reaction shown in (C).

Hepes, and 5 mM Ches to provide for control of ionic strength at approximately 50 mM and to provide for buffering within the pH* (see below) region of 5–10. Tetraethylammonium perchlorate (Eastman Chemicals) was recrystallized 4 times from hot water before use. Mes, Hepes, and Ches buffers were obtained from Sigma and were used as provided. Ultrapure divalent cation perchlorates were obtained from Alfa Products or Aldrich. Standard solutions of these salts were prepared by weight.

In spite of the precautions described above and the use of acid-washed glassware throughout (sulfuric/nitric, 3:1 v/v), the methanol/water solutions were found by atomic absorption measurements to contain unacceptable amounts of contaminating metals. The solutions were, therefore, routinely deionized by passage over a "Chelex 100" (Bio-Rad Laboratories) column. The resin was converted to the tetraethylammonium form prior to use. To accomplish the conversion, the resin was equilibrated with 1 N HCl, washed to a neutral effluent with distilled, deionized water, equilibrated with 1 N tetraethylammonium hydroxide, and again washed with water until a neutral effluent was obtained. After further equilibration of the resin with 80% methanol/water, 100 g wet weight of resin was utilized per liter of solution containing buffers and tetraethylammonium perchlorate as described above. Following deionization, the pH was adjusted to the desired value by the addition of reagent-grade perchloric acid (Fisher Scientific) or tetraethylammonium hydroxide (Eastman Chemicals), and the solutions were stored in polyethylene containers.

Nonaqueous pH Determination. Measurements of pH* in methanol/water mixtures were carried out by using a glass electrode (Corning 476022) in combination with a polymer body reference electrode (Markson 528-5114). Electrodes were equilibrated against aqueous standard buffers (Fisher Scientific, "Gram Pac") prior to equilibration with the methanol/water solutions. The operational pH* scales developed by de Ligny et al. (1960a,b) and Gelsema et al. (1966, 1967) were then utilized to determine the value of pH*. The term pH* is defined as $-\log a_H^*$, where a_H^* is the activity of H^+ in the mixed solvent. The term pH* when used in reference to a specific methanol/water mixture, therefore, has the same meaning as the term pH when used in reference to an aqueous solution [see Rorabecher et al. (1971) and references cited therein].

Data Acquisition and Analysis. All spectroscopic measurements were made at 25.0 °C. Absorption spectra were recorded on a Beckman DU-8 UV–vis spectrophotometer, whereas fluorescence spectra were obtained on an SLM 8000 spectrofluorometer operated in the analog mode and with correction for variations in source intensity as a function of wavelength. The spectra were not otherwise corrected. A Schott KV 390 filter was used in front of the fluorescence emission monochromator to improve the separation between fluorescence and scattered light. Both instruments were interfaced to microcomputer systems to allow for manipulation and plotting of the data.

In this report, equilibrium constants are reported for reactions of the type described by eq 1 and 2:

$$M^{2+} + A^- \rightleftharpoons MA^+ \quad (1)$$

$$MA^+ + OH^- \rightleftharpoons MA{\cdot}OH \quad (2)$$

In logarithmic form, the equilibrium expressions for reactions 1 and 2 are given by eq 3 and 4, respectively:

$$\log K_{MA} = pM + \log ([MA^+]/[A^-]) \quad (3)$$

$$\log K_{MA{\cdot}OH} = -\log [OH^-] + \log ([MA{\cdot}OH]/[MA^+]) \quad (4)$$

In these expressions, MA^+ refers to the 1:1 complex between the carboxylate anion of A23187 (M^-) and a divalent cation (M) while H^+ and OH^- have their usual meaning.

In many cases, it was not possible to determine the equilibrium constant for the reaction given by eq 1 directly. For some cations, the stability constants are too large, while for others the 2+ oxidation state is unstable, or insoluble metal hydroxides are formed at the pH* values required to minimize protonation of the ionophore. Therefore, pH*-dependent or "apparent" stability constants, K_{MA}', were determined in slightly acidic media (pH* $\simeq$5–6). The relationship between the pH*-independent and apparent stability constants is given by eq 5:

$$\log K_{MA} = \log K_{MA}' - \log \alpha_A \quad (5a)$$

where

$$\alpha_A = [A^-]/([A^-] + [HA]) = K_a/(K_a + a_H^*) \quad (5b)$$

[1] Abbreviations: Ches, 2-(*N*-cyclohexylamino)ethanesulfonic acid; Hepes, *N*-(2-hydroxyethyl)piperazine-*N*'-2-ethanesulfonic acid; Mes, 2-(*N*-morpholino)ethanesulfonic acid; HA, the free acid of A23187; A^-, the carboxylate anion of A23187; MA^+, a 1:1 divalent cation/A23187 complex; MA_2, a 1:2 divalent cation/A23187 complex.

For $pH^* \lesssim pK_a - 2$, $\alpha_A \cong K_a/a_H{}^*$, and eq 5 may be rewritten

$$\log K_{MA} = \log K_{MA}' + pK_a - pH^* \quad (6)$$

In eq 5 and 6, K_a refers to the mixed-mode acid dissociation constant which is known from previous work (Kauffman et al., 1982).

The apparent equilibrium constants, K_{MA}, were resolved from titration data expressed as plots log ($[MA^+]/[HA]$) vs. pM. The best fit to the experimental data was obtained by the least-squares method. Ratios of complexed to uncomplexed ionophore at a given cation concentration were calculated by using the equation:

$$[MA^+]/[HA] = \frac{\Delta S_{obsd}/\Delta S_{max}}{1 - \Delta S_{obsd}/\Delta S_{max}} \quad (7)$$

where ΔS_{obsd} is the observed spectral change (absorption or fluorescence) compared to the value in the absence of metal and ΔS_{max} is the maximal change obtained at saturation.

When ΔS_{max} could not be obtained experimentally because of low binding affinity, interference by other reactions, etc., it was estimated by extrapolation of plots of $1/[M^{2+}]$ vs. $1/\Delta S_{obsd}$.

The equilibrium constants, $K_{MA\cdot OH}$, were resolved from pH titrations of the species MA^+ using methods analogous to those described for K_{MA}.

Results

Equilibria between A23187 and Zn^{2+} in Solutions of 80% Methanol/Water. Spectrophotometric titrations of A23187 with Zn^{2+} at selected values of pH* are shown in Figure 2. It is apparent from these data that at least three equilibria between the cation and ligand are present within the range of conditions employed in these experiments. At pH* 5.00, the initial additions of Zn^{2+} produce the most marked spectral change near 278 nm. Isosbestic points are seen near 261, 294, and 372 nm. As the concentration of Zn^{2+} is increased further, a second equilibrium is indicated by the fact that the spectral changes at 278 nm approach completion while the absorbance at the 261- and 294-nm isosbestic points begins to increase. In addition, a new isosbestic point is seen near 283 nm. These same general features are seen when the titration is conducted at pH* 5.50; however, at pH* 6.00, new features indicating a third equilibrium are observed. Initial additions of Zn^{2+} still produce the most marked spectral change near 278 nm. However, as this first equilibrium approaches saturation, subsequent additions of Zn^{2+} fail to substantially enhance the absorbance at the 294-nm isosbestic point in the fashion seen at the lower values of pH*. Instead, the absorbance is enhanced in the region of 320–340 nm. This enhancement becomes more prominent as the pH* is increased to 6.50, 7.00, and 7.50. Within this more basic region of pH*, higher concentrations of Zn^{2+} produce spectra which have an isosbestic point at 306 nm which is not shared with the spectra obtained at lower concentrations of the cation.

It is not possible to extend these experiments to higher values of pH* since $Zn(OH)_2$ formation is already apparent in the pH* 7.50 data and is a more significant problem as the OH^- concentration is further increased (data not shown). It is also impractical to work below pH* ~5, because noncomplexing buffers with appropriate pK_a properties are not generally available. Thus, for studies with Zn^{2+}, we are confined to the pH* region covered in Figure 2, and the data indicate that at least three equilibria between the ionophore and Zn^{2+} are present over this range of conditions.

Insight into the identity of the three equilibria is obtained from Figure 3 which shows the fractional absorbance change at 278 nm as a function of Zn^{2+} added and at different values of pH*. At pH* 5.00, the complex(es) formed upon addition of substoichiometric amounts of Zn^{2+} is (are) not stable enough to reveal the Zn^{2+}/ionophore stoichiometry. However, at pH* 5.50, it is clear that the lowest levels of Zn^{2+} produce one or more species with a Zn^{2+}/ionophore stoichiometry of greater than 1:1. At pH* 6.00, the data are consistent with the first equilibrium representing formation of a 1:2 Zn^{2+}/ionophore complex as are the data obtained at pH* 6.50 and 7.00. A careful examination of these "end-point" plots shows either that the apparent stability of the initial 1:2 complex decreases slightly as the pH* is increased from 6.0 to 7.0 (improbable) or that increasing the OH^- concentration progressively favors a 1:1 complex compared to the 1:2 species. At pH* 7.50, this effect is more apparent. The initial additions of Zn^{2+} produce fractional absorbance changes which clearly lie closer to the line expected for stoichiometric formation of a 1:1 species.

The data in Figures 2 and 3 are consistent with the equilibrium model that follows: in the more acidic pH* region, additions of Zn^{2+} at well less than an amount stoichiometric with respect to A23187 results predominantly in formation of the species ZnA_2 according to reaction 8:

$$2HA + Zn^{2+} \rightleftharpoons ZnA_2 + 2H^+ \quad (8)$$

Reaction 8 is, of course, composed of the stepwise reactions 9 and 10.

$$HA + Zn^{2+} \rightleftharpoons ZnA^+ + H^+ \quad (9)$$

$$ZnA^+ + HA \rightleftharpoons ZnA_2 + H^+ \quad (10)$$

As reaction 8 approaches completion, further additions of Zn^{2+} result in conversion of the 2:1 complex to the 1:1 complex as shown by eq 11:

$$ZnA_2 + Zn^{2+} \rightleftharpoons 2ZnA^+ \quad (11)$$

This model requires that the equilibrium constant for reaction 10 is greater than or equal to that for reaction 9 (see below) in order to explain how ZnA_2 can persist in the presence of excess Zn^{2+}.

The third equilibrium, seen progressively as pH* is increased above approximately 6, is likely to be formation of the species ZnA·OH according to reaction 12 and/or reaction 13 depending upon conditions of Zn^{2+} concentration and pH*:

$$ZnA_2 + OH^- \rightleftharpoons ZnA\cdot OH + A^- \quad (12)$$

$$ZnA^+ + OH^- \rightleftharpoons ZnA\cdot OH \quad (13)$$

To support the model represented by eq 8–13, the effects of pH* on the spectrum of the species ZnA^+ were ascertained. Plots of absorbance at 294 nm vs. Zn^{2+} concentration (not shown) indicate that when the concentration of free Zn^{2+} is 2 mM or higher, the reaction represented by eq 11 is at least 95% complete, essentially isolating ZnA^+ from ZnA_2 or HA. When the ionophore, in the presence of this large excess of Zn^{2+}, is titrated with OH^-, the data shown in Figure 4 are obtained. A single well-behaved isosbestic point is observed (Figure 4A), the double-reciprocal plot is linear (Figure 4B), and the plot of log $[ZnA\cdot OH]/[ZnA^+]$ vs. $-\log [OH^-]$ is linear and displays a slope of −1.0 (Figure 4C). These findings are strong support for the existence of the species ZnA·OH and for the formation of this species by reaction 12 and/or 13 representing one of three equilibria seen in Figure 2. The log stability constant for formation of ZnA·OH as defined by eq 4 was determined to be 7.65.

To further support the equilibrium model, we considered the possibility that the initial spectral changes seen during the titrations were referable to the formation of ZnA_2H^+ as well

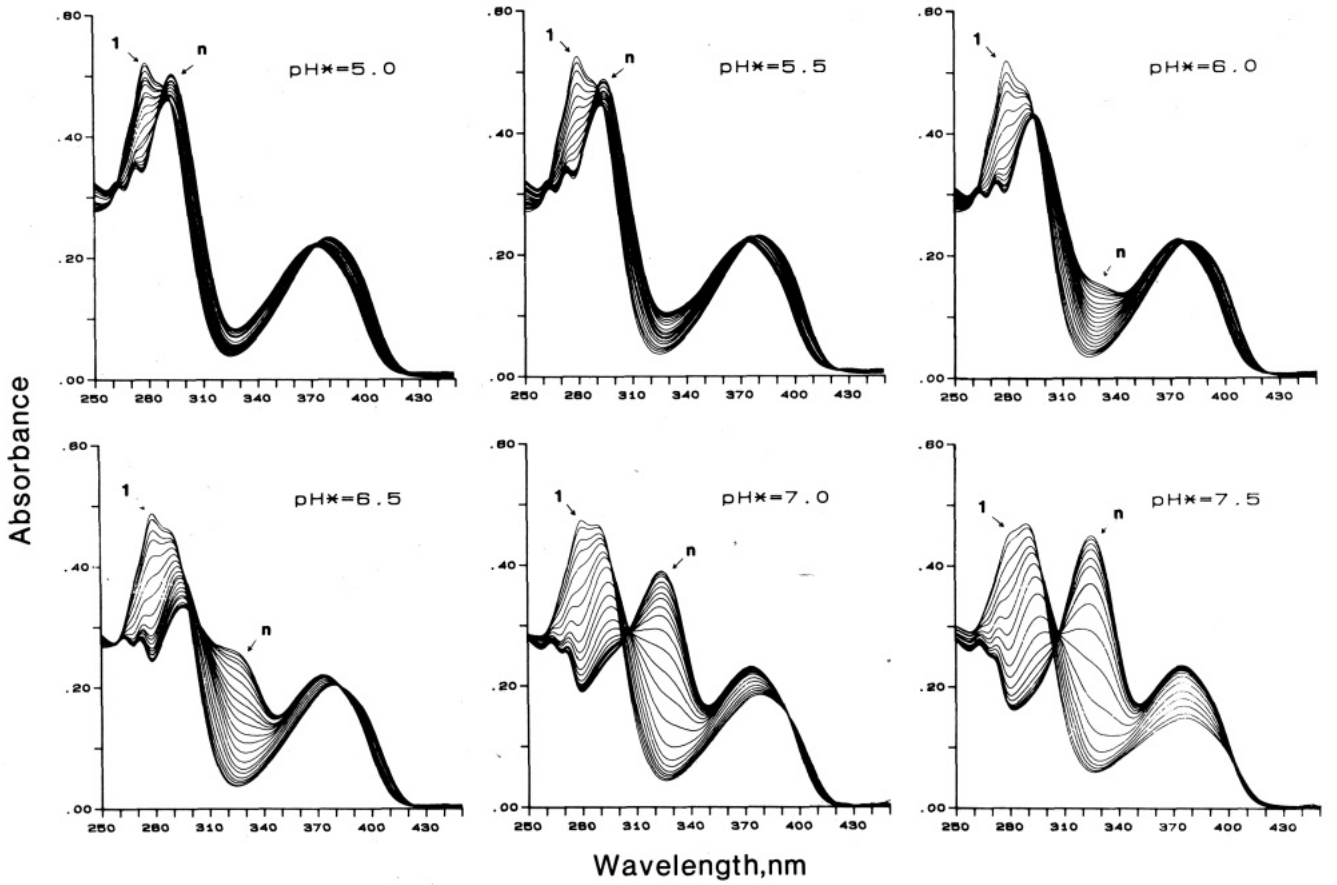

FIGURE 2: Absorbance titrations of A23187 with Zn^{2+} at selected values of pH*. Spectra were obtained in 80% methanol/water containing 33 mM tetraethylammonium perchlorate and 5 mM each of Mes, Hepes, and Ches. The concentration of A23187 was 25 μM, and the temperature was 25 °C. pH* was adjusted to the values indicated in the individual panels by using the procedures for nonaqueous pH determination described under Materials and Methods. $Zn(ClO_4)_2$ was added at appropriate concentrations in small volumes of the solvent solution. In each panel, the spectrum labeled 1 is that of the ionophore in the absence of Zn^{2+}, whereas the one labeled n is the spectrum observed at the highest Zn^{2+} concentration tested. Considering the spectral region near 278 nm, the initial additions of Zn^{2+} (less than stoichiometric with respect to A23187) produced a progressive decrease in absorbance. The reader is referred to Figure 3 and to the associated section of Results for a further description of the Zn^{2+} concentration range utilized in these titrations.

as to ZnA_2. Potentiometric titrations were conducted together with the absorption measurements so that moles of H^+ released per mole of Zn^{2+} complexed could be estimated. At the relatively low ionophore concentrations, the values obtained were not better than ±10%. Nevertheless, within this deviation, no evidence for the occurrence of ZnA_2H was obtained (data not shown).

Comparison of Equilibria between A23187 and Selected Divalent Cations. To determine if the equilibria observed between A23187 and Zn^{2+} represent interactions which occur generally between this ionophore and divalent cations, the data shown in Figure 5 were obtained. The transition series cations Ni^{2+}, Co^{2+}, and Mn^{2+} are complexed with an affinity similar to that of Zn^{2+} (see below), and titrations with these cations could be conducted at relatively acidic pH*. At pH* 6.00, these three cations produce the same types of spectral changes which are observed with Zn^{2+} at slightly lower values of pH* (compare the Ni^{2+}, Co^{2+}, and Mn^{2+} panels of Figure 5 with the pH* 5.0 and 5.5 panels in Figure 2). Using the data at 278 nm, end-point plots show the predominance of complex with the stoichiometry MA_2 (Figure 6, left). Increasing the cation concentration beyond the equivalence point for the first equilibrium results in increasing absorbance at the isosbestic point which is located near 295 nm and which is referable to the formation of the MA_2 species. Thus, with all of the transition series cations tested, the MA_2 species can undergo a disproportionation reaction analogous to eq 11.

When titrating with Zn^{2+} at pH* 6.00, the occurrence of reaction 12 and/or reaction 13 was already indicated by data in the 320–340-nm region (see Figure 2). Neither Ni^{2+}, Co^{2+}, nor Mn^{2+} gives the same evidence for formation of MA·OH at this (or more acidic) value of pH*; however, formation of NiA·OH and CoA·OH was apparent at higher pH* (data not shown). Using the conditions employed for Figure 4, it was not possible to get a good estimate of the stability constant for formation of these species because $Ni(OH)_2$ and $Co(OH)_2$ interference was encountered at pH* values less than those required to observe a measurable degree of formation of the ionophore/hydroxide-mixed complex. With Mn^{2+}, even above pH* 7.0, the hydroxide-related absorbance band in the 320–340-nm region was not observed, possibly indicating (see below) no significant occurrence of MnA·OH.

The alkaline earth cations tested are complexed by A23187 with substantially less affinity than the first transition series cations (Pfeiffer & Lardy, 1976; Young & Gomperts, 1977; Pfeiffer & Deber, 1978). Therefore, titrations were conducted at pH* 10.0 to eliminate the binding competition between cations and H^+. Figure 5 and Figure 6, right panel, show data obtained with Ca^{2+}, Mg^{2+}, and Sr^{2+}. Ca^{2+} and Mg^{2+} form MA_2 complexes, and with Mg^{2+}, the subsequent formation of MgA^+ according to eq 11 is clearly seen. The complexes formed with Sr^{2+} are not stable enough to allow estimation of their stoichiometry. With this cation as well as with Ca^{2+}, metal hydroxide formation began interfering before it could be determined if reactions 11, 12, and/or 13 were also occurring.

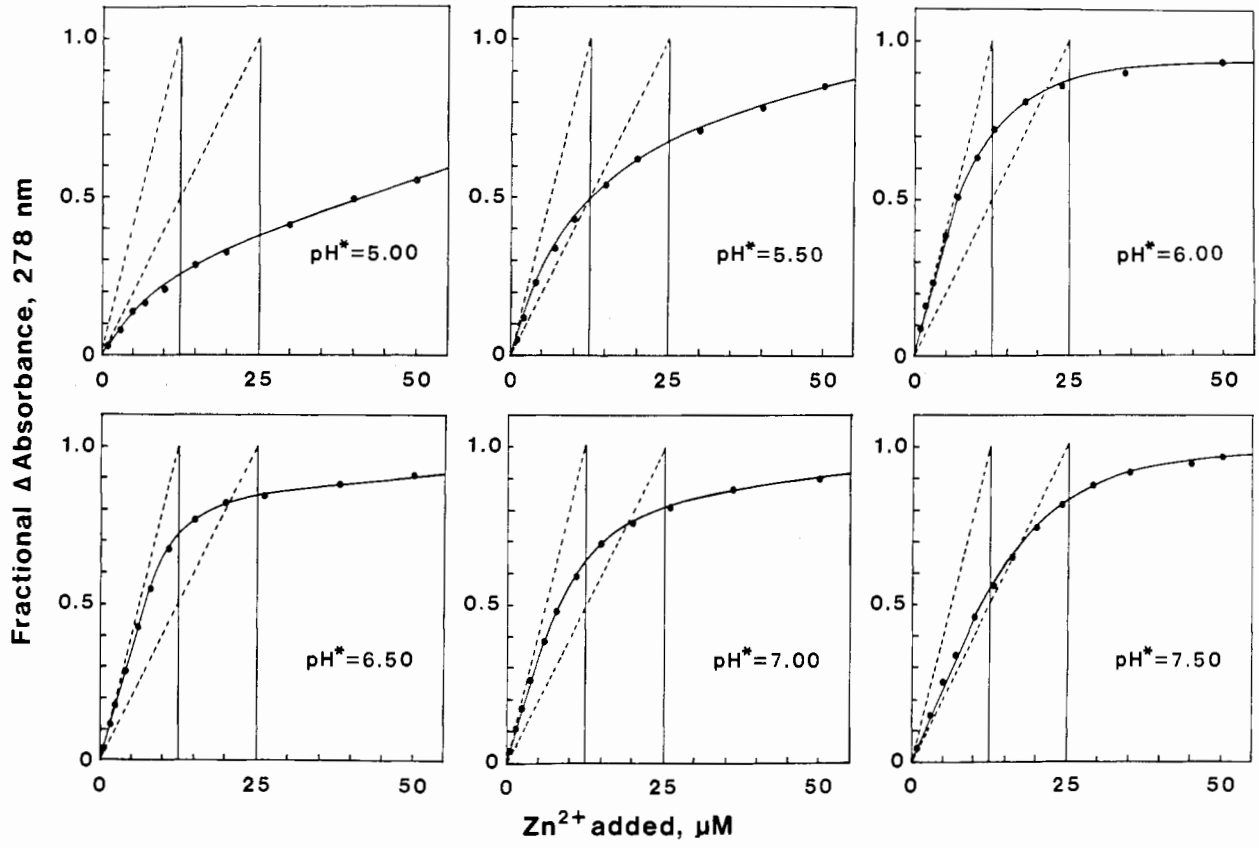

FIGURE 3: Fractional absorbance changes at 278 nm as a function of Zn^{2+} concentration and of pH*. The data were obtained from the spectra shown in Figure 2 at 278 nm and were converted by calculation to the fractional values shown. Each panel shows the equivalence point for the 1:2 and 1:1 complexes at 12.5 and 25 μM Zn^{2+}, respectively, as solid vertical lines extending from the Zn^{2+} concentration axis to a fractional absorbance value of 1.0. One of the two dashed lines, extending from the origin to the vertical lines, would contain all titration points if the initial additions of Zn^{2+} were bound stoichiometrically as one or the other of the two complexes.

Determination of Stability Constants for 1:1 Complexes (MA^+). To obtain a full description of the transport scheme shown in Figure 1, it will be necessary to obtain stability constants for all reactions given by eq 8–13. In principle, it is possible to isolate reaction 9 from the other equilibria by titrating the ionophore at concentrations which are low enough to ensure that formation of the MA_2 is negligible and at concentrations of OH^- below those where reaction 13 can interfere. Such experiments are possible with A23187 because the compound is strongly fluorescent, the fluorescence properties are altered by protonation or the complexation of cations, and the proton or metal binding affinities of the first excited state (as observed by fluorescence) are not significantly different from the values of the ground state (as observed by absorbance) [see Kauffman et al. (1982) and Taylor et al. (1985)].

A fluorescence titration of 30 nM A23187 with Zn^{2+} is shown in Figure 7A. In this particular experiment, the pH* was 5.80. Since the carboxylate protonation constant of the ionophore in this solvent is 7.85 ± 0.05 (Kauffman et al., 1982), more than 99% of the free ionophore exists in the protonated form, and the species A^- need not be considered as a reactant. This concentration of A23187 was selected as a practical lower limit for the determination of stability constants because of background fluorescence which was observed in the reagent solutions utilized. Fluorescing impurities contributed 10% or less of the total signal in this and subsequent experiments, with the exact value being a function of the free metal ion concentration present. Titration data were routinely corrected for background contributions by running a blank titration and subtracting those data from the data obtained in the presence of ionophore. When these precautions are taken, plots of reciprocal fluorescence change vs. the reciprocal Zn^{2+} concentration are linear (Figure 7B), indicating that complex formation has the expected first-order dependence on the free cation concentration. In addition, when the data are expressed as a plot of log $[ZnA^+]/[HA]$ (using eq 7) vs. pZn, the relationship is also linear and displays a slope of −1.0 (Figure 7C). These findings support the notion that at 30 nM A23187, reaction 9 is isolated from the other potential equilibria (see below for a further discussion of this point).

Data analogous to Figure 7 were obtained for several divalent cations across the pH* region of 5–6. The results are shown in Figure 8. For all cations, the relationship between log K_{MA}' and pH* is linear and displays a slope of 1.0, as predicted by reaction 9 and eq 6. By use of eq 6, the pH*-independent stability constant can be calculated from the data shown in Figure 8. These values, together with the previously determined values for H^+ and monovalent cations, are given in Table I.

Discussion

The data presented here indicate that equilibria between A23187 and divalent cations are more complex than is apparent from previous work. Earlier studies in methanol with Ca^{2+} and Mg^{2+} (Tissier et al., 1979; Krause et al., 1983) and with trivalent lanthanide cations (Albin et al., 1984) have shown that relatively low ratios of cation to A23187 result predominantly in species of the stoichiometry MA_2, whereas high ratios produce the 1:1 species. A more recent study has shown that the same situation pertains in solvents as polar as 70% methanol/water (Tissier et al., 1985). While the present work extends the earlier efforts to include the first-row transition metal divalent cations, it also shows for the first time,

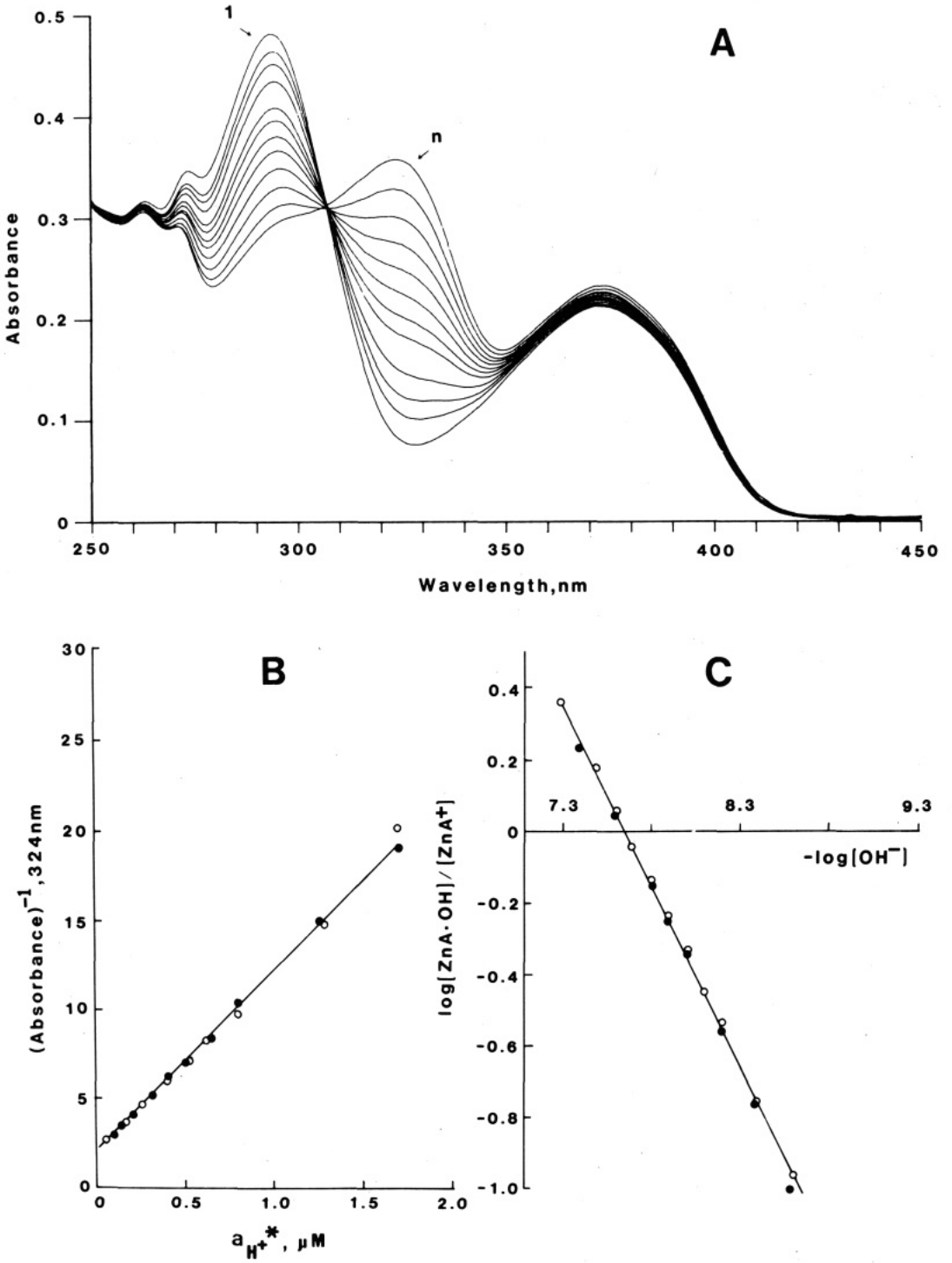

FIGURE 4: Determination of log $K_{ZnA\cdot OH}$ by absorbance titration. (Panel A) 25 μM A23187 in 80% methanol/water containing 2.0 mM $Zn(ClO_4)_2$ plus tetraethylammonium perchlorate and buffers as described in the legend to Figure 1 was titrated with tetraethylammonium hydroxide. pH* was varied from 5.00 (spectrum 1) to 6.81 (spectrum n). The temperature was 25 °C. (Panel B) The reciprocal absorbance at 324 nm is plotted as a function of H^+ activity to illustrate linearity and the identification of the maximum absorbance change (ΔS_{max}) at the y-axis intercept (an H^+ activity of 0 is equivalent to an infinite OH^- activity). (Panel C) By use of an expression analogous to eq 7, the data have been plotted according to eq 4. The –log [OH^-] values were calculated from the measured quantities, a_{H^+}*, by using 14.49 as –log of the solvent ionization constant (Koskikallio, 1957) and 0.65 as the activity coefficient of OH^- under the solution conditions employed. The latter value was obtained by using the extended Debye–Hückel equation, as described by Nancollas (1966). log $K_{ZnA\cdot OH}$ is equal to –log [OH^-] at log [ZnA·OH]/[ZnA^+] = 0. Open and closed symbols in panels B and C are data from two separate experiments.

that ionophore/hydroxide-mixed complexes (species of the type MA·OH) exist and are likely to be encountered in solution studies under conditions which are thought to be germane to the ionophore's transport properties.

From the present work, it is clear that the mixed ionophore/hydroxide complexes exist with the cations Zn^{2+}, Ni^{2+}, and Co^{2+}. For these cations, formation of the hydroxide adduct is indicated by a shift of the absorbance band near 300 nm in the spectra of 1:1 complexes to approximately 330 nm (see Figures 2 and 4). From previous assignments (Pfeiffer et al., 1974), it is the $\pi \rightarrow \pi^*$ transition of the α-ketopyrrole moiety (see Figure 1) which is undergoing this substantial red shift, while the lowest energy transition of the benzoxazole chromaphore, centered near 370 nm, is relatively unaffected. If this shift is taken as the indicator of mixed complex formation, it would appear at first that the ionophore/hydroxide

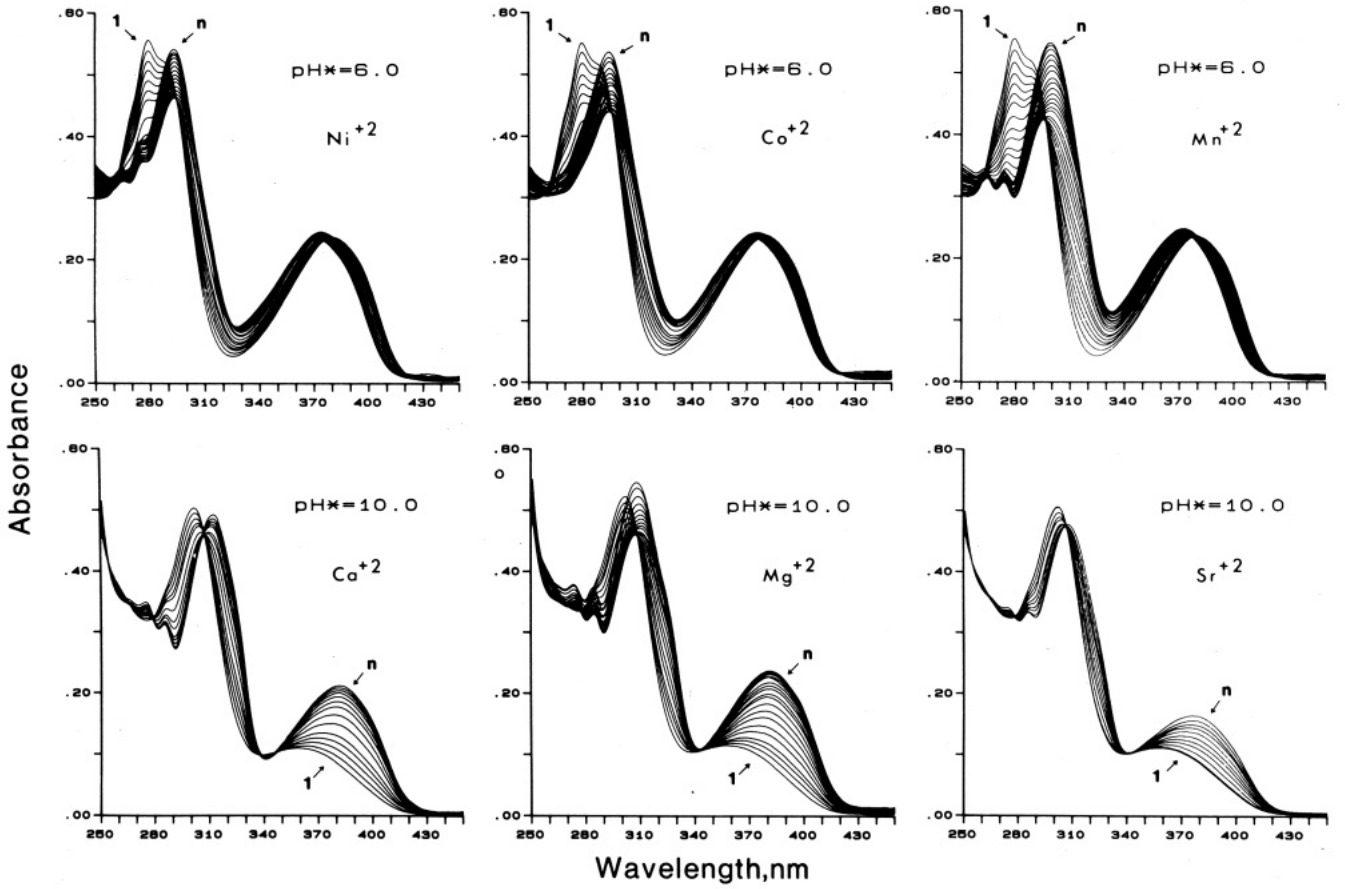

FIGURE 5: Absorbance titrations of A23187 with various divalent cations. Divalent metal perchlorates were used in all cases. Conditions were otherwise as described in the legend to Figure 2 except that the pH* values indicated in the individual panels were employed. The labeling of spectra and the trend of the titrations are also as described for Figure 2. With Ni^{2+}, Co^{2+}, Mn^{2+}, and Mg^{2+}, the experiments covered a cation concentration range of 0–~10 mM. With Ca^{2+} and Sr^{2+}, the experiments were terminated at cation concentrations too low to complete the reactions due to the onset of insoluble metal hydroxide formation.

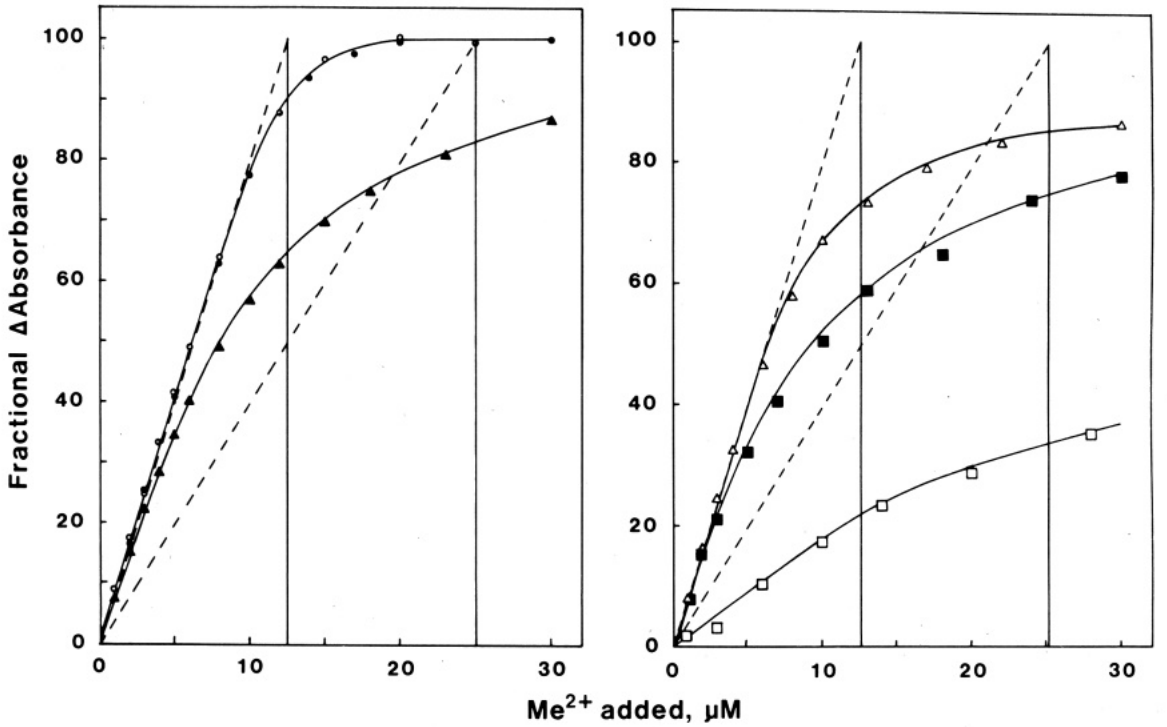

FIGURE 6: Fractional absorbance changes as a function of cation concentration. The data were obtained from the spectra shown in Figure 5. The solid vertical and dashed lines identify potential "end-point titration" behavior for formation of 1:2 or 1:1 complexes at the ionophore concentration employed (25 μM) as described in the legend to Figure 3. Left-side panel: (○) Ni^{2+}; (●) Co^{2+}; and (▲) Mn^{2+}. Values were calculated from the absorbance at 278 nm. Right-side panel: (△) Ca^{2+}; (■) Mg^{2+}; and (□) Sr^{2+}. Values were calculated from the absorbance at 380 nm.

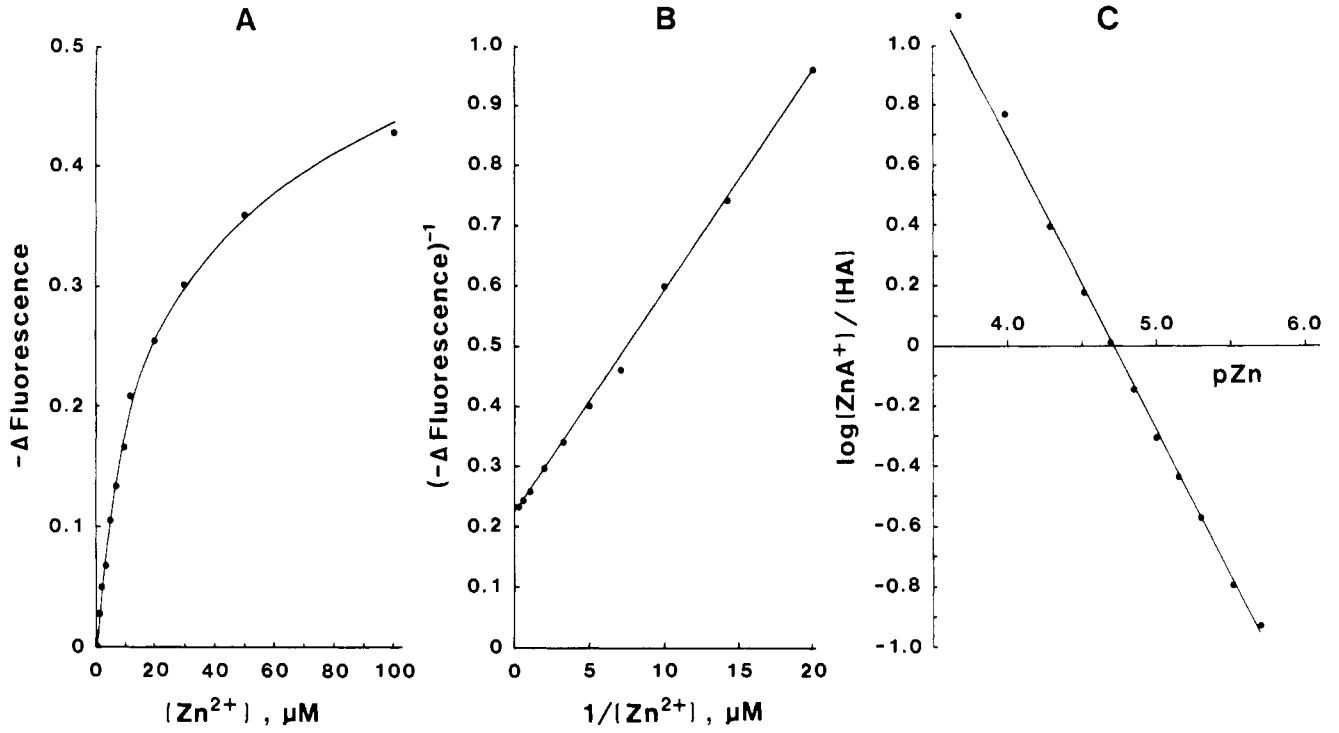

FIGURE 7: Determination of log K_{ZnA^+} by fluorometric titration. 30 nM A23187 in 80% methanol/water containing tetraethylammonium perchlorate and buffers as described in the legend to Figure 1 was titrated with $Zn(ClO_4)_2$ employing excitation and emission wavelengths of 365 and 435 nm, respectively. pH* was 5.80, and the temperature was 25 °C. (Panel A) The change in relative fluorescence as a function of Zn^{2+} concentration. These data have been corrected for the apparent fluorescence of reagent impurities by conducting a titration in the absence of ionophore, utilizing identical experimental and instrumental conditions, and subtracting the fluorescence values obtained for those observed in the presence of ionophore. In the experiment shown, this background fluorescence was 6% or less of the total fluorescence signal. (Panel B) The data are expressed as a double-reciprocal plot to demonstrate linearity and to illustrate the identification of the maximal fluorescence change at the y-axis intercept. (Panel C) The data have been plotted according to eq 3. log K_{ZnA^+} is equal to pZn at log $[ZnA^+]/[HA]$ = 0.

Table I: Known Stability Constants for 1:1 Complexes between A23187 and Cations in 80% Methanol/Water[a]

cation	log K_{MA}'	log K_{MA}
H^+		7.85 ± 0.05
Ni^{2+}	5.54 ± 0.02	7.54 ± 0.06
Co^{2+}	5.07 ± 0.03	7.07 ± 0.06
Zn^{2+}	4.79 ± 0.05	6.79 ± 0.07
Mn^{2+}	4.08 ± 0.03	6.08 ± 0.06
Mg^{2+}	2.55 ± 0.02	4.55 ± 0.05
Ca^{2+}	2.50 ± 0.02	4.50 ± 0.05
Sr^{2+}	1.86 ± 0.04	3.86 ± 0.06
Ba^{2+}	1.60 ± 0.04	3.60 ± 0.06
Li^+		3.08 ± 0.05
Na^+		2.36 ± 0.07

[a] All values were determined at 25.0 °C and at an ionic strength of approximately 50 mM. The value for H^+ is taken from Kauffman et al. (1982) whereas the values for Li^+ and Na^+ are from Taylor et al. (1985). log K_{MA}' values are pH* dependent and were determined at pH* 5.85. They represent stability constants for reactions of the type $M^{2+} + HA \rightleftharpoons MA^+ + H^+$. The standard deviations on these values and on log K_{MA} for H^+, Li^+, and Na^+ were obtained from five replicate determinations. log K_{MA}' values have been converted to the pH*-independent values log K_{MA} (defined by eq 3)] through use of eq 6. The standard deviations on these values were calculated according to the theory of error propagation and include the error in log K_{HA} as well as log K_{MA}'.

species is not significantly populated with the alkaline earth cations or with Mn^{2+}. As shown in Figure 5 (for Ca^{2+}, Mg^{2+}, and Sr^{2+}) or in data not shown (for Mn^{2+}), by the time the M^{2+} and OH^- concentrations have been raised to the point where interference by $M(OH)_2$ begins, the 300-nm absorbance band has not clearly begun to shift to the 330-nm region. However, these cations are more weakly bound than Ni^{2+}, Co^{2+}, and Zn^{2+}, and in general, reactions 8 and/or 11 are not completed before $M(OH)_2$ interference is encountered. If the red shift of the 300-nm absorbance band in the spectra of MA·OH complexes with alkaline earth cations and Mn^{2+} is less than that with Ni^{2+}, Co^{2+}, and Zn^{2+}, it could be difficult to distinguish between the formation of MA^+ and MA·OH by our present approach. By performing simultaneous potentiometric and absorbance titrations of A28187/Mg^{2+} mixtures at relatively acidic values of pH*, and in a solvent similar to that used here, Tissier et al. (1985) were able to estimate the absorbance spectrum of MgA^+ by calculation. Interestingly, their approach indicates that the 300-nm band should be located near 290 nm rather than near 310 nm as indicated by data in Figure 5. Since their calculated spectrum would be derived from measurements at relatively acidic pH* and is blue shifted compared to the observed spectrum at pH* 10 (Figure 5), it is possible that the second equilibrium seen with Mg^{2+} in Figure 5 is, in fact, the formation of MgA·OH. Although it may prove experimentally difficult to distinguish between formation of MA^+ and MA·OH with cations of physiological interest, it seems important to do so because the latter species is charge neutral and might be another transporting species of this ionophore.

As pointed out under Results, we will ultimately require stability constants for all reactions given by eq 8–13 to interpret the transport properties of A23187 quantitatively. Regarding reactions 8–11, where formation of a mixed ionophore/hydroxide complex is not involved, the present data show that constants for reaction 8 would be difficult to obtain directly because the MA_2 species are too stable under pH conditions of interest (see Figures 3 and 6) and because reactions 8 and 11 are commonly overlapping. It would also be difficult to directly determine the constants for reactions 9 and 10 by

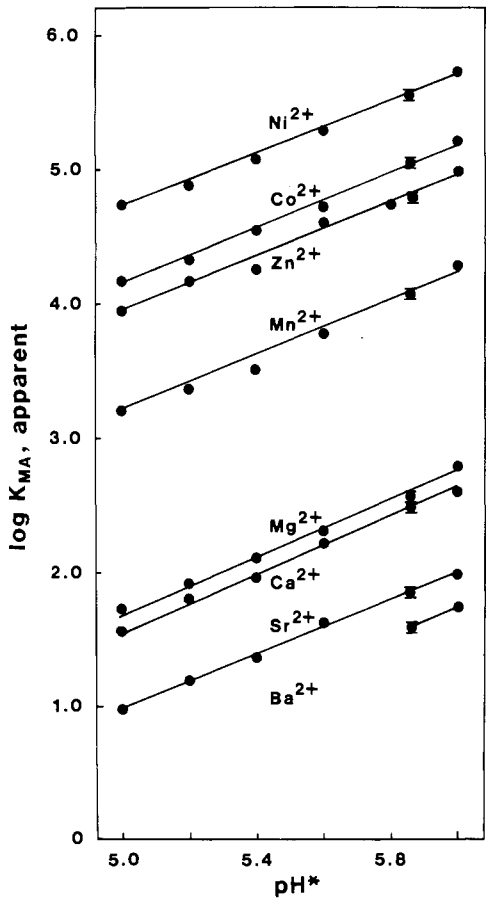

FIGURE 8: Effect of pH* on $K_{MA}{}'$ for selected divalent cations. Experiments analogous to Figure 7 were conducted over a range of pH* and with various divalent cations as indicated in the figure. The perchlorate salts were employed for all cations investigated. The values presented for pH* 5.85 are the mean ± SD of five replicate determinations. Other values are from single determinations.

techniques and under experimental conditions which could be used with phospholipid membrane containing systems. However, it is possible to calculate the constants for reactions 8 and 10 if those for reactions 9 and 11 can be measured with precision. Figures 7 and 8 indicate that by using low concentrations of the ionophore and fluorescence spectroscopy to monitor the reactions, reliable values for reaction 9 can be directly obtained. To determine how effectively the use of 30 nM A23187 isolates the formation of MA^+ from MA_2 (reaction 9 from reaction 10), we utilized the "COMICS" program (Perrin & Sayce, 1967) to simulate the distribution of A23187 between the two species under conditions of interest. When we assumed a log stability constant for formation of the 1:1 complex similar to the value determined for Ni^{2+} and then calculated how much MA_2 would exist at various values of log K_{MA_2}, M^{2+} concentration, and pH, no significant population of the MA_2 species was predicted when log $K_{MA_2} \simeq$ log K_{MA} even at neutral pH and at a low M^{2+} concentration (2 μM), typical of the initial values employed in these titrations. If log K_{MA_2} = log K_{MA} + 1 and 2 μM M^{2+} was assumed, no significant MA_2 occurs at pH 5, whereas only 3.6% and 8.6% of total ionophore existing as the 1:2 species is expected at pH 6 and 7, respectively. These small proportions of MA_2 are gone at 600 μM M^{2+}, a concentration which is typical of that present near the completion of these titrations. As the estimates or log K_{MA_2} were increased further, the simulated distributions showed that at the beginning of titrations (low M^{2+} concentration), the formation of MA_2 would increasingly interfere with the determination of log K_{MA}, particularly at high pH values. In contrast, if log $K_{MA} \simeq 4.5$ was assumed (similar to the values determined for Ca^{2+} and Mg^{2+}), the accumulation of MA_2 never became very significant, even when log K_{MA_2} = log K_{MA} + 3 (complete results not shown).

These simulations confirmed that interference by MA_2 formation with the determination of log K_{MA} (as was done in Figures 7 and 8) is greatest for the tightly bound cations at the higher values of pH* employed and increases as log K_{MA_2}/log K_{MA} increases. It is doubtful that K_{MA_2} exceeds K_{MA} by much more than a factor of 10 for any of the cations studied here. This is indicated by previous estimates of these values for Ca^{2+} and Mg^{2+} (Tissier et al., 1979) and by using the data in Figures 2 and 5 to estimate the equilibrium constants for reaction 11 and then calculating approximate values of K_{MA_2} (not shown). In addition, for a second stepwise binding constant to exceed the first value by more than a factor of 10 is rare in complexation chemistry. Thus, in Figure 8, it is the Ni^{2+} data, near pH* 6, which are the "worst case" with respect to isolating reaction 9 from reaction 10, and it is probable than even with these data, the formation of MA_2 is not significant.

Further support for the accuracy of the 1:1 constants obtained at low ionophore concentration has been obtained from kinetic studies of the Ni^{2+}–A23187 complexation–dissociation reactions in 80% methanol/water solvent (T. P. Thomas and R. W. Taylor, unpublished results). A value of log K_{NiA} = 7.63 ± 0.05 was obtained by this independent approach ($K_{NiA} = k_{form}/k_{diss}$) which is in excellent agreement with the value of 7.54 ± 0.05 (see Table I) obtained by fluorometric titration.

The values of K_{MA} reported here can be compared to previously reported values in other solvents and to apparent overall constants obtained by the two-phase extraction technique. For Ca^{2+} and Mg^{2+}, the present values in 80% methanol/water are very similar to those found in 70% methanol/water (Tissier et al., 1985) but are approximately 2 orders of magnitude lower than those seen in 90% methanol/water (Tissier et al., 1985) and 3 orders lower than in methanol (Tissier et al., 1979, 1985; Bolte et al., 1982). Thus, the stability of 1:1 complexes rises sharply as the solvent methanol content exceeds 80% but does not diminish rapidly at lower methanol contents. This behavior is similar to the effect of solvent composition on the ionophore protonation reaction (Kauffman et al., 1982; Tissier et al., 1985) and is in contrast to the relative insensitivity of K_{MA} to this parameter with monovalent cations (Taylor et al., 1985).

Two-phase extraction constants, which reflect the overall stability of the species MA_2, were reported previously for the same set of cations studied here (Pfeiffer & Lardy, 1976; Pfeiffer & Deber, 1978). Those values showed a simple pattern as a function of ionic radius, with ZnA_2 being the most stable and log stability constants decreasing rapidly and linearly with ionic size for larger or smaller cations. By comparison, the formation constants for the 1:1 complexes reported here indicate an altered and diminished binding selectivity. In the 1:2 complexes, cations are located in a binding cavity that is not easily distorted and is, therefore, size selective. Part of the rigidity arises from conformational constraints on the individual ionophore molecules in the dimeric structure and from the fact that the two molecules interact by hydrogen bonds (Deber & Pfeiffer, 1976; Pfeiffer & Deber, 1978). In 1:1 complexes, these conformational constraints are greatly diminished. However, the stability constants for the 1:1 complexes follow the order predicted by Irving and Williams (1953) when expanded to include the alkaline earth cations (Vallee & Coleman, 1964). The trend exhibited is similar to those observed for other simple carboxylate-containing chelating ligands such as oxalic acid (Martell & Smith, 1977)

and quinoline-2-carboxylic acid (Martell & Smith, 1974). Thus, the binding selectivity observed for the 1:1 complexes arises, in large part, from the "hard and soft" qualities (Pearson, 1968) of the metal ions and ligand donor atoms (Siegel & McCormick, 1970).

Finally, the present results give additional insights into the properties of this ionophore which should be considered when interpreting its transport activities and biochemical effects. Regarding biochemical effects, the data reemphasize that the affinity of A23187 for trace metals found in biological systems far exceeds its affinity for Ca^{2+} and Mg^{2+}. Thus, ionophore-catalyzed transport of trace metals should be considered possible, even when systems contain much higher concentrations of Ca^{2+} and Mg^{2+}. Regarding transport data, the unusual relative magnitudes of stepwise binding constants for the formation of MA_2 ($K_{MA_2} \simeq 10K_{MA}$) can be seen as favorable to formation of the transporting dimeric species in the presence of excess cation. Nevertheless, it is clear for cations studied here that increasing the cation concentrations will ultimately promote formation of nontransporting MA^+ with a parallel decline in transport rate. This factor has not always been considered in previous studies on the transport properties of this compound.

References

Albin, M., Cader, B. M., & Horrocks, W. DeW., Jr. (1984) *Inorg. Chem. 23*, 3045–3050.

Bates, R. G., Paabo, M., & Robinson, R. A. (1963) *J. Phys. Chem. 67*, 1833–1838.

Bolte, J., DeMuynck, C., Jeminet, G., Juillard, J., & Tissier, C. (1982) *Can. J. Chem. 60*, 981–989.

Chaney, M. O., Demarco, P. V., Jones, N. D., & Occolowitz, J. L. (1974) *J. Am. Chem. Soc. 96*, 1932–1933.

Deber, C. M., & Pfeiffer, D. R. (1976) *Biochemistry 15*, 132–141.

de Ligny, C. L., Luykx, P. F. M., Rehbach, M., & Weineke, A. A. (1960a) *Recl. Trav. Chim. Pays-Bas 79*, 699–712.

de Ligny, C. L., Luykx, P. F. M., Renbach, M., & Weineke, A. A. (1960b) *Recl. Trav. Chim. Pays-Bas 79*, 713–726.

Gelsema, W. J., de Ligny, C. L., Remijnse, A. G., & Blijleven, H. A. (1966) *Recl. Trav. Chim. Pays-Bas 85*, 647–660.

Gelsema, W. J., de Ligny, C. L., & Blijleven, H. A. (1967) *Recl. Trav. Chim. Pays-Bas 86*, 852–864.

Hamill, R. L., Gorman, M., Gale, R. M., Higgins, C. E., & Hoehn, M. M. (1972) 12th International Conference on Antimicrobial Agents and Chemotherapy, Atlantic City, NJ, Abstr. 32.

Irving, H., & Williams, R. J. P. (1953) *J. Chem. Soc. 156*, 3192–3210.

Kauffman, R. F., Taylor, R. W., & Pfeiffer, D. R. (1982) *Biochemistry 21*, 2426–2435.

Kauffman, R. F., Chapman, C. J., & Pfeiffer, D. R. (1983) *Biochemistry 22*, 3985–3992.

Koskikallio, J. (1957) *Suom. Kemistil. B 30*, 111–114.

Kruase, G., Grell, E., Albrecht-Gary, A. M., Boyd, D. W., & Schwing, J. P. (1983) in *Physical Chemistry of Transmembrane Ion Motions* (Spach, G., Ed.) pp 255–263, Elsevier, Amsterdam.

Martell, A. E., & Smith, R. M. (1974) in *Critical Stability Constants*, Vol. 1, p 372, Plenum Press, New York.

Martell, A. E., & Smith, R. M. (1977) in *Critical Stability Constants*, Vol. 3, pp 92–95, Plenum Press, New York.

Nancollas, G. H. (1966) in *Interactions in Electrolyte Solutions*, pp 13–14, Elsevier, New York.

Pearson, R. G. (1968) *J. Chem. Educ. 45*, 581–587.

Perrin, D. D., & Sayce, I. G. (1967) *Talanta 14*, 833–842.

Pfeiffer, D. R., & Lardy, H. A. (1976) *Biochemistry 15*, 935–943.

Pfeiffer, D. R., & Deber, C. M. (1979) *FEBS Lett. 105*, 360–364.

Pfeiffer, D. R., Reed, P. W., & Lardy, H. A. (1974) *Biochemistry 13*, 4007–4014.

Pfeiffer, D. R., Taylor, R. W., & Lardy, H. A. (1978) *Ann. N.Y. Acad. Sci. 307*, 402–423.

Reed, P. W., & Lardy, H. A. (1972) *J. Biol. Chem. 247*, 6970–6977.

Rorabacher, D. G., MacKellar, W. J., Shu, F. R., & Bonavita, S. M. (1971) *Anal. Chem. 43*, 561–573.

Sigel, H., & McCormick, D. B. (1970) *Acc. Chem. Res. 3*, 201–208.

Taylor, R. W., Kauffman, R. F., & Pfeiffer, D. R. (1982) in *The Polyether Antibiotics: Naturally Occurring Acid Ionophores* (Westley, J. W., Ed.) Vol. 1, pp 103–184, Marcel Dekker, New York.

Taylor, R. W., Chapman, C. J., & Pfeiffer, D. R. (1985) *Biochemistry 24*, 4852–4859.

Tissier, C., Julliard, J., Dupin, M., & Jeminet, G. (1979) *J. Chim. Phys. Phys.-Chim. Biol. 76*, 611–617.

Tissier, C., Juillard, J., Boyd, D. W., & Albrecht-Gary, A. M. (1985) *J. Chim. Phys. Phys.-Chim. Biol. 82*, 899–906.

Vallee, B. L., & Coleman, J. E. (1964) *Compr. Biochem. 12*, 165–177.

Young, S. P., & Gomperts, B. D. (1977) *Biochim. Biophys. Acta 469*, 281–291.